Ion Channel Pharmacology Under Flow: Automation Via Well-Plate Microfluidics

C. Ian Spencer,[1,] Nianzhen Li,[1] Qin Chen,[1] Juliette Johnson,[1] Tanner Nevill,[1] Juha Kammonen,[2,†] and Cristian Ionescu-Zanetti[1]*

[1]Fluxion Biosciences, Inc., South San Francisco, California.
[2]Pfizer Global Research and Development, Sandwich, United Kingdom.
**Present address: The Gladstone Institute of Cardiovascular Disease, San Francisco, California.*
[†]Present address: Pfizer Neusentis, Cambridge, United Kingdom.

ABSTRACT

Automated patch clamping addresses the need for high-throughput screening of chemical entities that alter ion channel function. As a result, there is considerable utility in the pharmaceutical screening arena for novel platforms that can produce relevant data both rapidly and consistently. Here we present results that were obtained with an innovative microfluidic automated patch clamp system utilizing a well-plate that eliminates the necessity of internal robotic liquid handling. Continuous recording from cell ensembles, rapid solution switching, and a bench-top footprint enable a number of assay formats previously inaccessible to automated systems. An electro-pneumatic interface was employed to drive the laminar flow of solutions in a microfluidic network that delivered cells in suspension to ensemble recording sites. Whole-cell voltage clamp was applied to linear arrays of 20 cells in parallel utilizing a 64-channel voltage clamp amplifier. A number of unique assays requiring sequential compound applications separated by a second or less, such as rapid determination of the agonist EC_{50} for a ligand-gated ion channel or the kinetics of desensitization recovery, are enabled by the system. In addition, the system was validated via electrophysiological characterizations of both voltage-gated and ligand-gated ion channel targets: $hK_V2.1$ and human Ether-à-go-go–related gene potassium channels, $hNa_V1.7$ and 1.8 sodium channels, and (α1) $hGABA_A$ and (α1) human nicotinic acetylcholine receptor receptors. Our results show that the voltage dependence, kinetics, and interactions of these channels with pharmacological agents were matched to reference data. The results from these IonFlux™ experiments demonstrate that the system provides high-throughput automated electrophysiology with enhanced reliability and consistency, in a user-friendly format.

INTRODUCTION

The patch clamp technique is known to provide accurate details on the conduction and gating properties of ion channels, yet its usefulness for drug discovery is limited by a characteristically slow data accumulation rate. Accordingly, several types of automated patch clamp (APC) systems have been devised to enable pharmaceutical laboratories to pursue ion channel targets at relatively high throughput.[1–5] In most of the commercial automated electrophysiology platforms, glass patch pipettes have been replaced by a planar substrate incorporating numerous holes of subcellular dimensions.[6–9] Cell capture by suction allows for many patch-clamping sites on the planar surface and simple perfusion systems have been replaced by fluid-handling robots. For higher throughput, whole-cell currents are summated from populations of captured cells, providing in-built signal averaging that greatly improves both the success rate and uniformity of recordings.[10]

In recent years, many investigations have validated APC data from a wide array of voltage- and ligand-gated ion channels, and few, if any, ion channel targets are inaccessible to these systems.[10–14] On the other hand, despite the widespread use of automated electrophysiology in the pharmaceutical industry, the available instruments tend to be costly, and retain systematic weaknesses that narrow the interpretation of results. In one example, the recording electrodes and compound-delivery pipettes must alternately occupy the same physical space, meaning that the cell membrane is not under voltage clamp for prolonged periods. In addition to creating other uncertainties, this unclamping happens crucially during compound additions precluding the study of most ligand-gated ion channels.[9,15] Other systems more closely emulate conventional patch clamp, but are forced to operate asynchronously to allow for the complex logistics of fluid handling in response to cells entering the whole-cell configuration at different times.[13,14] These obstacles reduce total throughput by creating scheduling difficulties for onboard liquid handlers being driven by the timeline of an experimental protocol. They also constrain the allowable timings of compound exchange, such that some instruments require at least 3 s between drug additions and prevent the user from performing more than eight synchronous compound additions due to reliance on an eight-channel pipettor design. Even where many pipettes are present in the fluidic

ABBREVIATIONS: APC, automated patch clamp; CHO, Chinese hamster ovary; CNS; DMSO, dimethyl sulfoxide; ECS, extracellular saline solution; ERA, ensemble recording array; GABA, γ-aminobutyric acid; HEK, human embryonic kidney; hERG, human *Ether-à-go-go*–related gene; $hGABA_A$, GABA receptor; hNAChR, human nicotinic acetylcholine receptor; ICS, intracellular solution; IV, current versus voltage; SBS, Society for Biomolecular Sciences; TEA, tetraethylammonium chloride.

DOI: 10.1089/adt.2011.414

head, there are necessary time delays between one addition and the next, placing constraints on what protocols maybe executed.

In this report we present results that were obtained with a novel, synchronous microfluidic patch clamp device. The IonFlux™ system utilizes microfluidic channels molded into a polymeric substrate. Cell membranes form robust seals at channels in the substrate, which is itself bonded to Society for Biomolecular Sciences (SBS) standard microwell plates to create self-contained consumables that are seamlessly compatible with external plate/liquid handlers.[16,17] The resulting compact systems require no electrical or mechanical isolation, enabling automated cell perfusion and recording. IonFlux plates are simultaneously addressed by up to 64 patch clamp amplifiers, together with an interface that uses air pressure to drive liquid translation. Since robot scheduling constraints are removed, any compound well can be pressurized at any time enabling synchronous compound additions across the plate without wait times between applications. This facilitates, for example, open-channel modulation of desensitizing ligand-gated ion channels that must be exposed to a second modulator compound shortly (<1 s) after an agonist addition. No bulk fluid handling occurs inside the instrument, providing great flexibility and simplicity. The IonFlux system is also the first bench-top APC system with a plate-reader form factor, and the first to incorporate temperature control at the patch sites.[18] Here we describe in detail the design and operation of the IonFlux instrument and we present our initial validation data obtained from a diverse set of heterologously expressed human ion channels.

METHODS

Cell Handling

The IonFlux instrument is designed to work primarily with suspensions of small cultured cells. To facilitate the present work, human ion channels heterologously expressed in human embryonic kidney (HEK-293) and Chinese hamster ovary (CHO) backgrounds were kindly provided by Millipore Corp. These PrecisION™ HEK cell lines expressed, respectively, hGABA$_A$ receptor (hGABA$_A$R) ($\alpha1\beta3\gamma2$), human nicotinic acetylcholine receptor (hNAChR) ($\alpha1\beta1\delta\varepsilon$), hNa$_V$1.7, and 1.8, and were specified by part numbers CYL 3068, 3052, 3011, and 3025, respectively. We also utilized CYL 3038, which expressed the human *Ether-à-go-go*–related gene (hERG) channel (CHO). Each PrecisION cell line was cultured according to the accompanying user guide, except in the case of hNa$_V$1.8, where gene expression was additionally boosted by adding 1 mM lidocaine hydrochloride to the culture medium to act as a chemical chaperone, followed by removal of the drug ~2 h prior to experiments.[19] A CHO cell line expressing hK$_V$2.1 was cultivated in standard low-glucose Dulbecco's modified Eagle's medium with 10% fetal bovine serum and the hK$_V$2.1 channels were induced no less than 4 h before experiments by adding 50 µg/mL of doxycycline hyclate to the medium.[20] Prior to electrophysiology studies, growth medium was removed from the culture flask and cells were washed once with prewarmed Ca^{2+}- and Mg^{2+}-free Dulbecco's phosphate-buffered saline (DPBS), which was replaced by 2–3 mL of a detachment agent (Accutase from Sigma-Aldrich Chem. Co., or Detachin from Gelantis) (also rinsed once) before transferring the flask back for 5 min to a 37°C (5% CO_2/humidified) incubator. Cells were collected by washing the flask with fresh, prewarmed medium or extracellular solution (ECS) and by triturating gently using a serological pipette to disaggregate any clumps. Cells were then separated from suspension by centrifugation at 200 *g* for 1.5 min, and were washed up to five times with fresh ECS to minimize cell debris in the final preparation. Cells were counted and the appropriate ECS volume was determined, giving ~2–5 million cells/mL for IonFlux experiments.

Electrophysiology

Voltage command protocols used in these studies are similar to those employed in conventional patch clamping as follows: (i) hGABA$_A$R (I_{Cl}) and hNAChR cation current (I_{Cat}) were activated by ligand binding at a steady holding potential (V_h) of −80 mV; (ii) hK$_V$2.1 current was evoked by 30-ms steps to +70 mV from V_h −80 mV; (iii) for hERG current, V_h was also −80 mV and an initial step to +50 mV for 800 ms inactivated the channels, followed by a 1-s step to −50 mV to elicit the outward tail current that was measured (the "50/50" protocol); (iv) for both hNa$_V$1.7 and 1.8, I_{Na} was evoked by depolarizing to −10 mV for 50 ms after a 100-ms step to −120 mV from V_h −90 mV. Stimulation frequencies were in the range of 0.2–1 Hz for the various voltage-gated currents.

The ability to specify the pressures applied to wells on the consumable plate as part of an experimental protocol is unique to the IonFlux instrument. As such, pneumatic pressures applied above the wells enable the translocation of cells and experimental solutions within the microfluidic network. The consumable is a triple sandwich made from a bottomless SBS standard 96- or 384-well plate and a punched and imprinted polymeric layer forming fluidic channels and microchannels when a flat, transparent polymer sheet provides a bottom for the channels.[17] The fluidic networks are arranged in experimental "patterns" comprised of sets of 12 wells (*Fig. 1*). Various wells in the pattern have differing functions: cells and ECS are placed into the inlet well, flowing over the recording sites in a main channel leading to the outlet well when headspace pressure is applied to inlet well. Upstream of the recording sites, eight fluidic channels branch laterally from the side wall of the main channel leading to wells supplying compound-containing solutions (compounds 1–8). The recording sites communicate with duplicate wells (traps 1 and 2) containing intracellular solution (ICS), also responsible for applying suction (when vacuum is applied above the well) to trap cells and achieve whole-cell voltage clamp. Recording sites themselves are termed ensemble recording arrays (ERAs) consisting of a comb-like arrangement of 20 individual microchannels, each of which captures a cell (*Fig. 1C*). Voltage clamp control is applied to the whole ERA via Ag/AgCl electrodes contacting the ICS (in trapping wells), while a reference electrode is situated in the inlet well of each zone. The recorded whole-cell current, therefore, is summated from all 20 cells captured by an ERA. The 384-well IonFlux consumable is contacted by 64 independent voltage clamp amplifiers. There are four experiment areas on the 384-well substrate; each has eight experimental zones with any zone providing a duplicate read-out of responses to

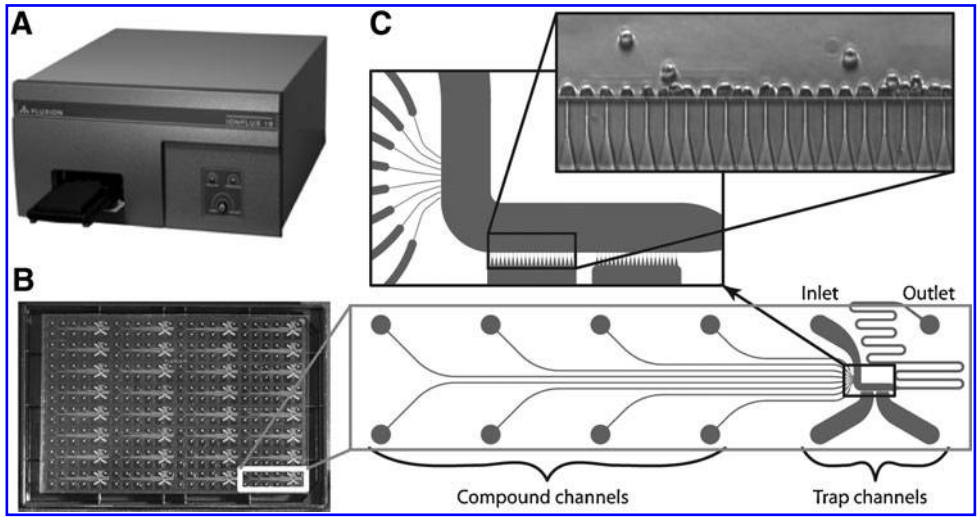

Fig. 1. The instrument layout. **(A)** Photograph of the IonFlux instrument, with a 384-well IonFlux consumable on the plate tray, ready to be drawn into the electro-pneumatic interface. **(B)** Digital photograph of the underside of the 384-well consumable; the 32 experimental patterns are clearly visible after introducing dye into the microfluidic network interconnecting the wells, mapped for one experimental zone (white box). **(C)** Schematic of the microfluidics for the experimental zone. Each experimental zone is an interconnected network of microfluidic channels **(***bottom, inset from* **B)** with inlets into a 12-well pattern (●). The 12-well pattern contains two trap channels, with wells and microfluidics containing ICS, that function to capture cells at the recording sites (black box). An inlet supplies cells plus ECS, and the outlet accumulates the flow-through waste. The remaining eight compound channels (C1–C8) supply compound-containing ECS. All compound channels converge just upstream of the ERA recording site. (*Inset*) Micrograph of an ERA, composed of 20 microfluidic channels occupied by captured cells. ECS, extracellular solution; ERA, ensemble recording array; ICS, intracellular solution.

the compounds contained in eight-compound channels. Any combination of experimental zones indicated in *Figure 1* can be filled with solutions for inclusion into a given experimental run.

The IonFlux experiment has four phases, each of which is specified in software in terms of well pressures, voltage applied to cells, and signals recorded (*Fig. 2A, B*). These phases are as follows: (i) priming the microfluidic channels, (ii) capturing cells in the ERA, (iii) establishing whole-cell recording (break-in), and (iv) data acquisition. For priming, positive pressure is applied to all wells, pushing the desired experimental solutions through the fluidic channels. The ratio of priming pressures applied to the microfluidic channels and main channels, respectively, is typically 7 pounds per square inch (~0.5 Bar, 50 kPa) to 1 p.s.i., ensuring that all solutions flow through the system to the outlet well. During this phase, series resistance (R_s) is monitored using a train of ~20 mV voltage steps, and the junction potential between ICS and ECS is corrected automatically, by applying a voltage offset. Cells are captured from the ECS suspension by applying a negative pressure of around 5 inches of mercury (~0.2 Bar, 20 kPa) to the trapping wells, leading to full occupancy of the ERA in under 30 s. Additional suction applied during the break-in phase ruptures the cell membrane across the mouths of the microchannels, and suction can be maintained throughout the experiment.

The contaminating effects of R_s and capacitance currents can be compensated electronically. While complete series and capacitance current compensation is difficult to obtain for ensembles, certain minimum values (such as "pipette" resistance in the microfluidic network) can be easily compensated and improve overall voltage control. Data acquisition sweeps in response to predetermined voltage command protocols and compound applications are used to generate a real-time data plot displayed in software (*Fig. 2*). Data output and analysis are discussed below.

Leak resistance is measured by introducing at short 20 mV pulse (typically −80 to −100 mV) at the beginning of each sweep and measuring the current difference. Assuming linear leak, proportional currents are subtracted from each of the different voltage command segments. The same method is applied to both ligand- and voltage-gated channel recordings. R_s compensation is applied in order to cancel out the resistance of the microfluidics when recording from large conductance ion channels, such as Na^+ channels. R_s was measured in unoccupied microfluidic channels before cells were introduced into the system, and was found to vary slightly from channel to channel, between 0.5 and 0.7 MΩ. There are two user-selectable gain levels in the IonFlux system. For low-gain recordings (large currents, *e.g.*, $GABA_A$), root mean square (RMS) noise was on the order of 10–20 pA, dependent on cell type and seal quality. Currents can be measured from 5 pA (at high gain) to 400 nA (at low gain).

Solutions

Standard tissue culture reagents were as specified by Millipore Corp. with the substitution of media containing Glutamax™ (Gibco) instead of L-glutamine. Expressed channels were maintained by selection using G418, hygromycin B (Invitrogen 10131, 10687) and/or puromycin (Clontech 631306), with doxycycline hyclate used for inducing $K_V2.1$ (Sigma Aldrich; D9891). Unless otherwise stated, all reagents were purchased from Sigma Aldrich Co. A standard extracellular solution (ECS) was employed containing (in mM): NaCl, 137; KCl, 4; $MgCl_2$, 1; $CaCl_2$, 1.8; dextrose, 10; and HEPES, 20, corrected to pH 7.4 using NaOH. ICS differed by cell line. For experiments with $hGABA_A$ and hNACh (α1) receptors in HEK cells and with $K_V2.1$ CHO cells, ICS contained (in mM): K aspartate, 130; $MgCl_2$, 5; K_2EGTA, 5; TrisATP, 4; and HEPES, 10, corrected to pH 7.1 using KOH. For HEK

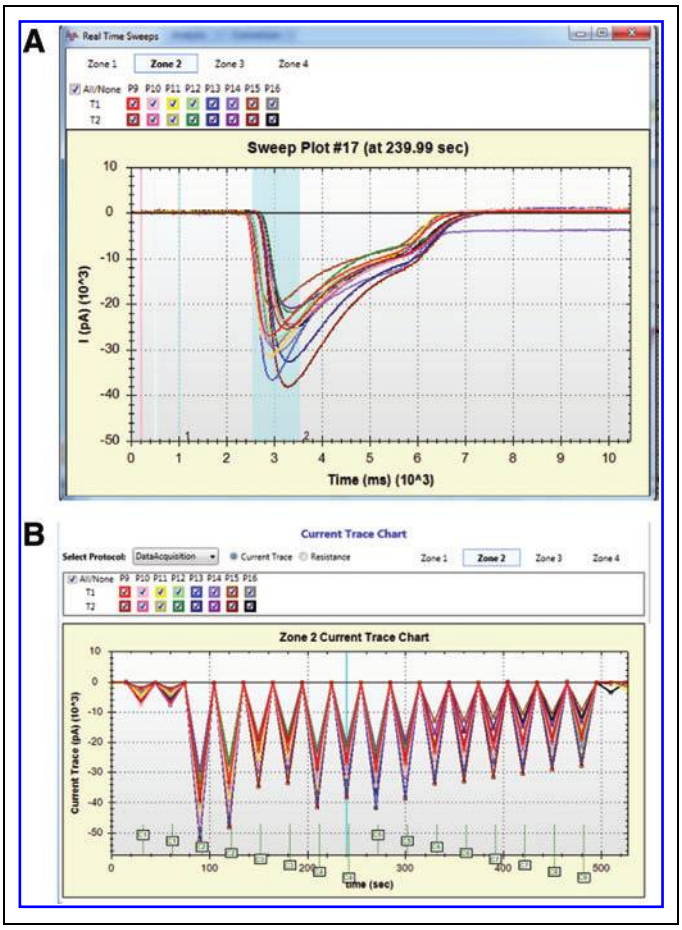

Fig. 2. Software and data presentation. The monitoring during data acquisition phases consists of two screens. A sweep window **(A)** displays the latest data sampling sweep with measurement cursors. The two cursors determine a current differential of interest that is plotted against overall elapsed time during the experiment in the current trace screen. Cursors are of variable width, to create running-average sweep monitoring if desired. An example sweep plot window is shown for the $hGABA_A$ receptor's inward I_{Cl}. The currents were centered at zero by automatic leak subtraction, and the negative (inward) deflections occurred when 5 μM GABA was applied. In the current trace chart **(B)**, differential current amplitudes are plotted as a function of time for repeated GABA additions. Each color represents an individual ERA channel, and annotated event markers can be used to show the precise timing of compound additions. GABA, γ-aminobutyric acid; $hGABA_A$, GABA receptor. Color images available online at www.liebertonline.com/adt

cells expressing $hNa_V1.7$ or 1.8, a fluoride-based ICS was used to increase the stability of recordings.[21] The composition was as follows (mM): CsF, 100; CsCl, 45; CsHEPES, 10; NaCl, 5; and CsEGTA, 5, corrected to pH 7.1 using CsOH. For CHO hERG cells, ICS consisted of (in mM): KCl, 120; K_2EGTA, 10; Na_2ATP, 4; $MgCl_2$, 1.75; $CaCl_2$, 5.4; and HEPES, 10, corrected to pH 7.1 using KOH. Finally, in some experiments determining the cumulative agonist dose–response experiments for HEK-$hGABA_A$ cells, ECS contained (in mM): NaCl, 140; Na gluconate, 5; KCl, 5; $MgCl_2$, 1; $CaCl_2$, 2; HEPES, 10, and glucose, 10, corrected to pH 7.4 with NaOH; and ICS contained: KCl, 120; EGTA, 10; $MgCl_2$, 1.75; $CaCl_2$, 4; CsF, 2; HEPES, 10; and Mg-ATP, 2, corrected to pH 7.2 with KOH. Note that a minimal well volume of 200 μL of ICS and ECS was required in electrode-containing wells to ensure contact with electrodes on the IonFlux 16 instrument.

Directly soluble pharmacological agents dissolved in ECS consisted of γ-aminobutyric acid (GABA), acetyl choline (ACh) isoguvacine HCl, tetraethylammonium chloride (TEA), quinidine HCl, and lidocaine HCl. All other reagents were solubilized in dimethyl sulfoxide (DMSO) in stock solutions at 10–50 mM, such that the total DMSO in any solution never exceeded 1%. All of the experimental solutions were dispensed into the wells of the IonFlux consumable plate immediately before running an experiment, although adhesive plate covers could be used for temporary storage of preloaded plates for extra convenience.

Data Handling

The IonFlux instrument features data sampling at frequencies from 1 to 20 kHz. In the experiments reported here, a sampling frequency of 10 kHz was employed for I_{Na}, hERG, and $K_V2.1$ currents, while ligand-gated I_{Cl} (GABA) and I_{Cat} (ACh) were acquired at 1 kHz. Data analysis software enables the immediate review and reduction of data from an experimental run. The data sweeps that generate a real-time current versus time plot (*Fig. 2A*) can be recalled to refine the cursor positions to improve the time course plot for final export, and to capture sweeps for overlay. Cursor measurements are reported as a function of time for the duration of the experiment (*Fig. 2B*). Data sweeps were generally exported into Microsoft Excel™ and, where necessary, curve fitting was performed using Origin™ (Origin Labs). For comparing apparent drug affinity, dose–response plots for relative current or block were fitted using the Origin™ built-in Hill equation (Hill coeficient: n_H).

RESULTS

$hK_V2.1$ Potassium Current

The upper panel of *Figure 3A* reproduces ensemble $hK_V2.1$ current ($I_{KV2.1}$) traces, showing relatively slow activation (~20 ms) and the absence of discernable inactivation (which is orders of magnitude slower than activation for this channel). The graph below shows the amplitude of $I_{KV2.1}$, measured between the baseline and steady level at the end of each voltage step, at 5-min intervals for all 16 ERA recording sites on a representative IonFlux plate. The longevity of $I_{KV2.1}$ was similar for 11/16 ensembles, with a mean amplitude of 16 ± 1 nA for the first 5 min and 14 ± 1 nA after 20 min of recording, a decrement of only 12.5%. The time course of most individual currents was invariant throughout the experiment (top). In five ensembles, however, $I_{KV2.1}$ ran down and, considering the whole plate, the mean $I_{KV2.1}$ at 5 min was 13 ± 1 nA with a median amplitude of 15 nA ($n = 16$). Further validation data, shown in *Figure 3B*, consist of the current versus voltage (IV) plot averaged over 10 rundown-free ERA channels, and its comparison with an equivalent IV plot from a

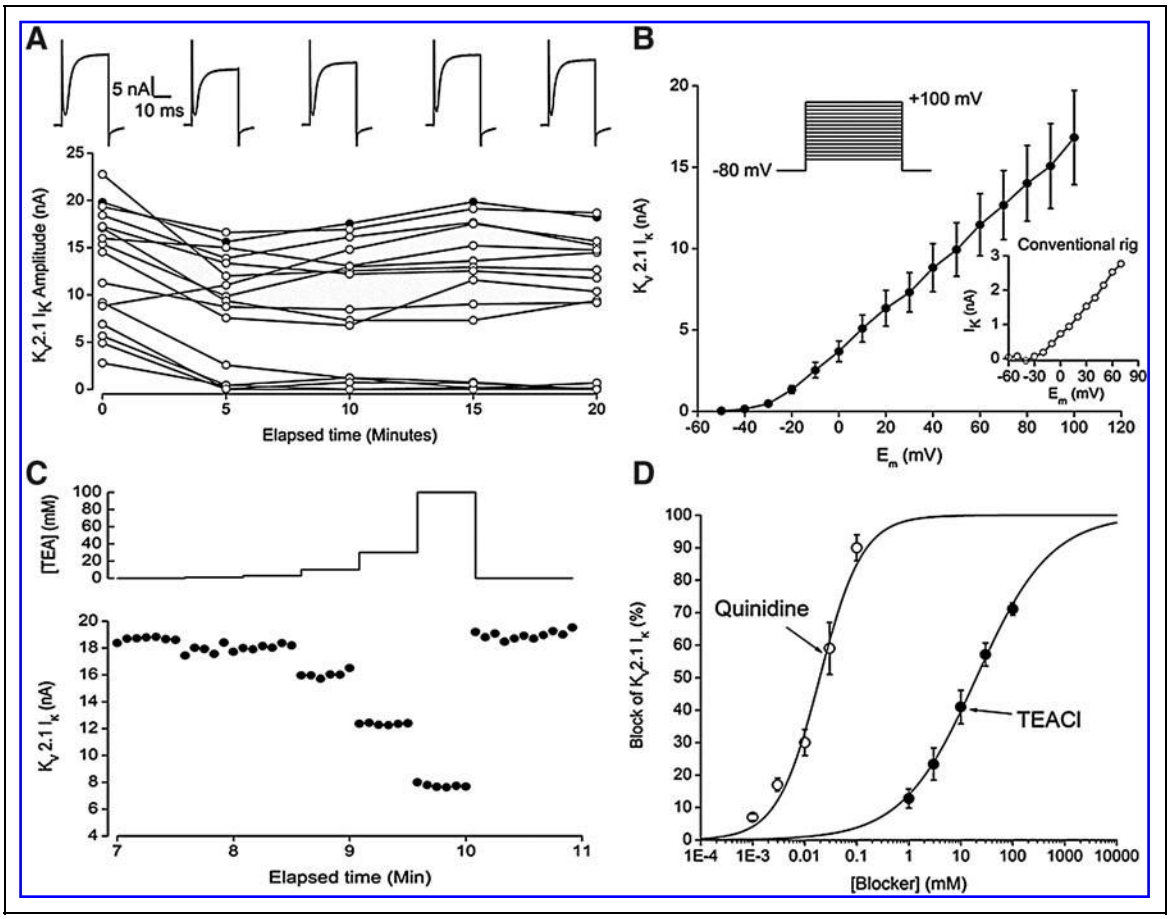

Fig. 3. hK_V2.1 potassium channel recordings. **(A)** Plot of the longevity of ensemble CHO-hK_V2.1 current amplitude, with samples at 5-min intervals, for all ensembles on one IonFlux consumable plate. V_{hold} −80 mV, V_{test} +70 mV (30 ms); pulse sequence applied at 0.2 Hz throughout. Actual current sweeps corresponding to the sweeps marking the 5-min intervals are shown above the graph for a representative ensemble, indicated in the plot by filled symbols. The *y*-axis reflects the amplitude of ensemble $I_{KV2.1}$, plotted against elapsed time. **(B)** Current versus voltage plot for mean ensemble hK_V2.1 potassium current recorded (n = 10 ensembles), with the voltage command family (V_{test} −80 to +100 mV, 30 ms) and data from a single cell in the equivalent conventional patch clamp experiment shown as insets. Note the increase in total current level resulting from summation of the currents from the ensemble cell population. **(C)** TEA block of hK_V2.1 current for a representative ensemble recording channel. The upper panel graphically represents the [TEA] applied cumulatively (with no washout between doses) from successive compound channels, while the lower plot shows peak $I_{KV2.1}$ (filled symbols) stimulated at a frequency of 0.2 Hz (5 s intervals) versus elapsed time. **(D)** Dose–response curves for percentage block of hK_V2.1 mean ensemble current by TEA^+ and quinidine with Hill fits to the data (see text for details). CHO, Chinese hamster ovary; TEA, tetraethylammonium chloride.

single, conventionally patch-clamped cell (inset). Both the takeoff potentials and slopes of these curves were very similar.

To investigate K_V2.1 pharmacology, ensemble $I_{KV2.1}$ was blocked using the known K^+ channel blockers, TEA and quinidine. *Figure 3C* presents graphically the time course of cumulative TEA^+ block for a typical IonFlux ERA. The range of [TEACl] applied from successive compound channels is shown in the upper panel, while the lower shows $I_{KV2.1}$ amplitude, plotted against elapsed time. Each step increase in [TEA] was accompanied by an immediate decrease in $I_{KV2.1}$, within a single 5-s stimulation interval, consistent with the rapid exchange of solutions available with microfluidics. The current was stable until the next TEA addition or washout of the blocker at the end. Note that washout was complete and very rapid because the small volume of the recording chamber and microfluidic delivery result in an exchange rate of roughly 10× the recording chamber volume per minute. *Figure 3D* compares the Hill fits to cumulative dose–response curves for TEA and quinidine block of $I_{KV2.1}$, revealing IC_{50} values of 20 ± 1 mM for TEA (n_H 0.61 ± 0.03, n = 10 ensembles) and 19.4 ± 2.5 μM for quinidine (n_H 1.1 ± 0.1, n = 6 ensembles). The assay success rate (defined as current exceeding a minimum of 2 nA for a protocol duration > 10 min) was 80% ± 4% across different eight experiments. Seal resistances (R_{seal}) averaged 200 MΩ/cell for the duration of the experiment (10 MΩ for 20-cells in parallel), although R_{seal} cannot be easily measured independently

of membrane resistance once cells in the ensemble start to enter whole-cell clamp.

hERG Potassium Current

Ensemble CHO-hERG currents typified by *Figure 4A* reproduced the known salient qualities of the underlying hERG channel, such as (i) the low current amplitude at positive membrane potentials (+50 mV) due to the kinetics of closed-state inactivation being faster than activation, (ii) a large outward tail current upon repolarization to a moderately negative potential (−50 mV) where hERG channels rapidly recover from inactivation before slowly deactivating, and (iii) a large inward tail upon further hyperpolarizing the membrane to −120 mV (not illustrated). The voltage dependence for activation of IonFlux ensemble hERG outward tail current (*Fig. 4B*) had a $V_{1/2}$ of ∼−4 mV, with slope factor of 12 similar to reference values (CYL3038 datasheet), and the current exhibited the expected rectification at potentials positive to −40 mV (*Fig. 4C*). Sample hERG tail current pharmacology data from IonFlux experiments are shown in *Figure 4D*, where Hill fits yielded IC_{50} values of 25 ± 1 nM (n_H 1.16 ± 0.04, n = 16 ensembles) for terfenadine, 58 ± 5 nM (n_H 1.24 ± 0.05, n = 14 ensembles) for cisapride, and 0.74 ± 0.13 μM (n_H 0.94 ± 0.05, n = 5 ensembles) for quinidine. Success rates (defined as hERG tail current >200 pA for the duration of a 30-min experiment, and decrement rate <2% per minute) averaged 77% over three control experiments performed. For these cells, R_{seal} varied from 60 to 1000 MΩ/cell ($R_{ensemble}$ = 3–50 MΩ), with an average of 350 MΩ/cell.

hNa$_V$1.7 and 1.8 Sodium Currents

In accordance with published findings, the ensemble HEK-hNa$_V$1.7 and 1.8 currents differed greatly in voltage dependence,

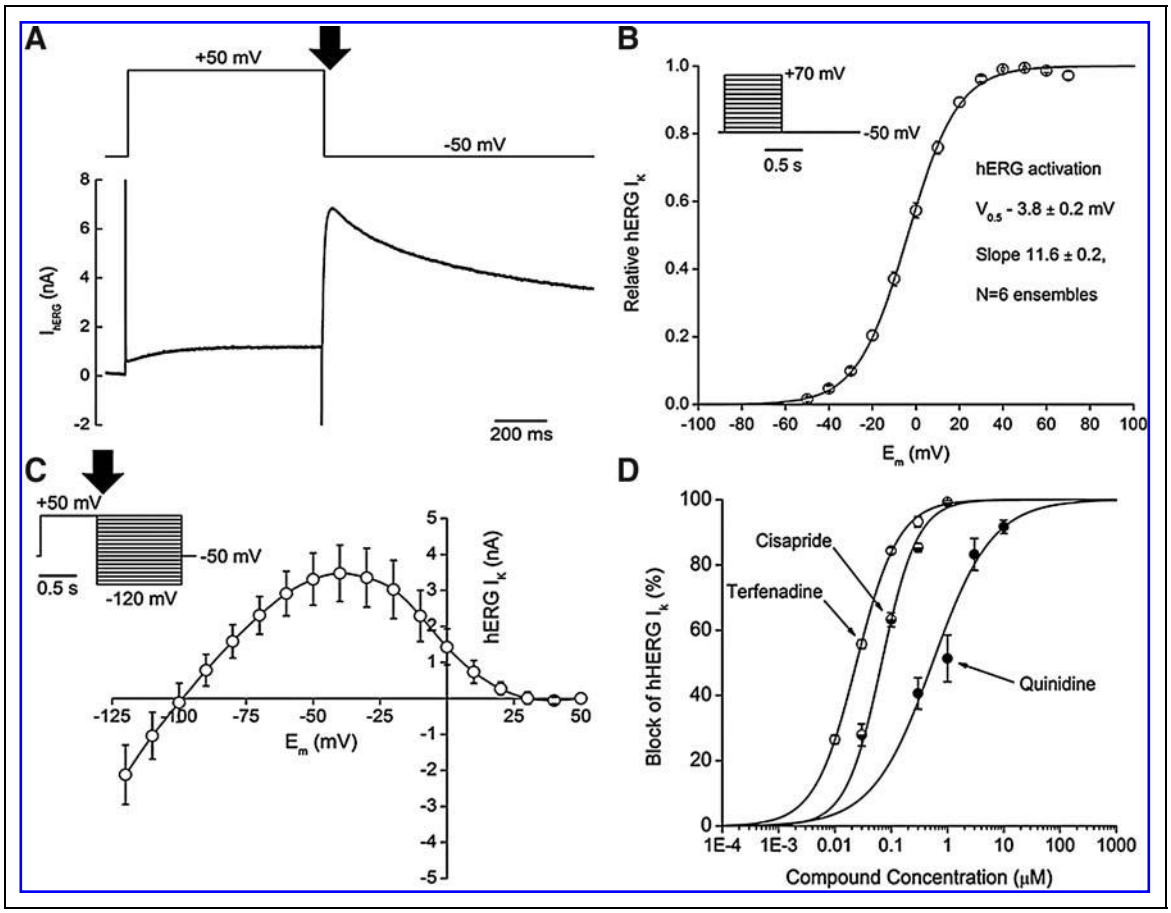

Fig. 4. CHO-hERG potassium channel recordings. **(A)** Sample recording of ensemble hERG current (lower trace) determined using the 50/50 voltage command protocol, shown schematically above the trace. All hERG voltage protocols were applied at 6-s intervals. **(B)** Mean activation voltage dependence for peak hERG tail current (in CHO cells) with the Boltzmann fit parameters displayed on the graph. The inset shows the voltage command protocol. **(C)** Mean plot for the fully activated IV relationship of the tail current, based on repolarization steps of variable magnitude as shown in the inset. This plot clearly reproduces the known rectification properties of the hERG channel. **(D)** Dose–response curves for block of peak ensemble outward tail hERG currents, obtained using the 50/50 protocol as in **(A)**. The curves show % block of outward tail current (measured at −50 mV; large arrows are voltage commands) and IC_{50}s calculated for terfenadine (25 ± 1 nM), cisapride (58 ± 5 nM), and quinidine (0.74 ± 0.13 μM) using Hill fits to the data. hERG, human *Ether-à-go-go*–related gene; IV, current versus voltage.

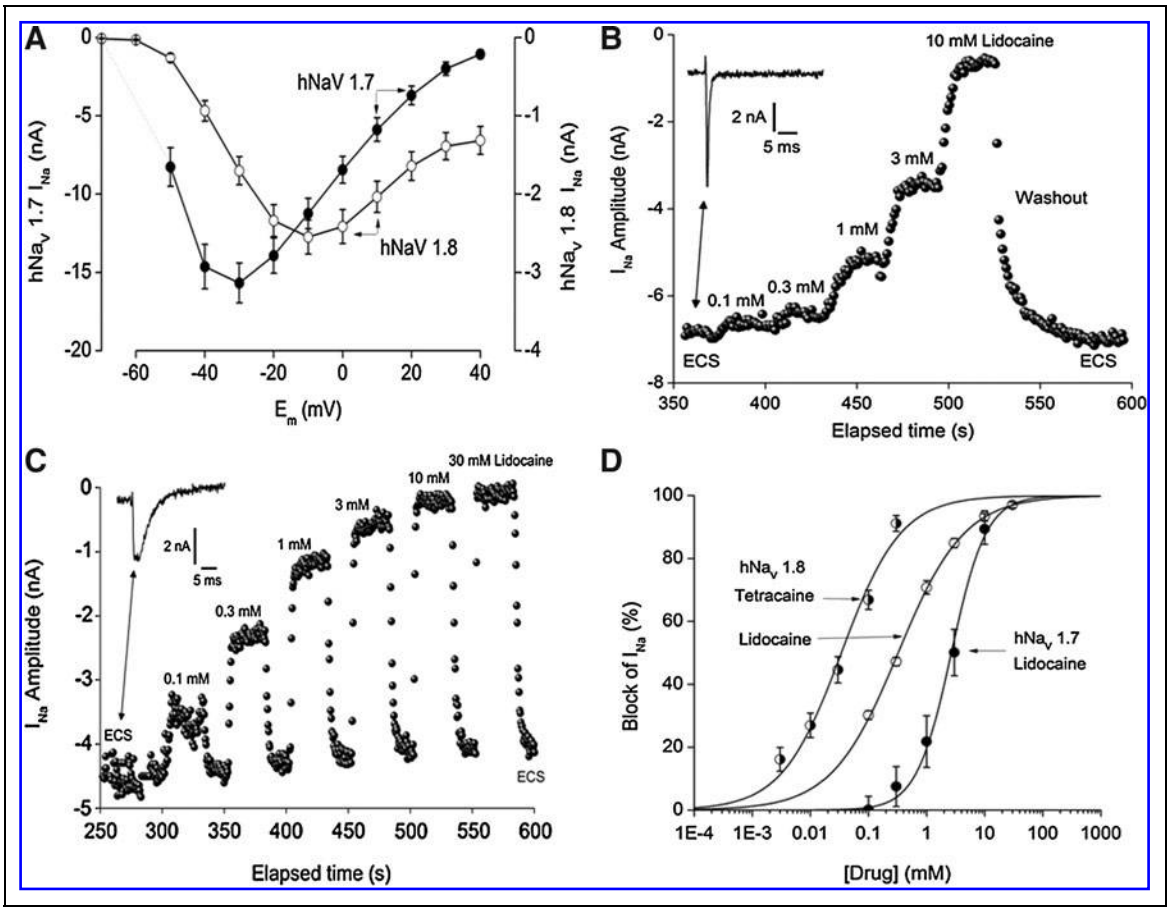

Fig. 5. HEK-hNa$_V$1.7 and hNa$_V$1.8 sodium channel recordings. **(A)** Superimposed IV plots for hNa$_V$1.7 (left axis) and 1.8 current (right axis). V_{hold} −80 mV, prestep to −120 mV (50 ms), and V_{test} −70 to +40 mV (50 ms). Pulse sequence applied at 1 Hz. **(B)** Plot of I_{Na} amplitude versus elapsed time during a cumulative dose–response experiment for Na$_V$1.7. Pulses are as in **(A)**, V_{test} −10 mV (duration 50 ms, frequency 1 Hz). Each lidocaine concentration was applied from a different compound channel, pressurized successively. (*Inset*) The difference current sensitive to 10 mM lidocaine for a representative ensemble recording. **(C)** Plot of I_{Na} amplitude versus elapsed time during a dose–response experiment for Na$_V$1.8, with transient washout of lidocaine between successive compound applications. Pulses as in **(A)**, V_{test} −10 mV (duration 50 ms, frequency 1 Hz). (*Inset*) The difference current sensitive to 30 mM lidocaine for a representative ensemble. **(D)** Dose–response plots for % block of hNa$_V$1.7 by lidocaine (filled symbols) and for block of hNa$_V$1.8 by lidocaine (open symbols) and tetracaine (half-filled symbols). The Hill fit parameters were as follows: for Na$_V$1.7 and lidocaine, IC_{50} 2.67 ± 0.23 mM (n_H 1.5 ± 0.1, n = 10); for Na$_V$1.8 and lidocaine, IC_{50} 0.32 ± 0.01 mM (n_H 0.8 ± 0.02, n = 16); and for Na$_V$1.8 and tetracaine, IC_{50} 0.034 ± 0.006 mM (n_H 0.9 ± 0.1, n = 35). HEK, human embryonic kidney.

peak amplitude, and kinetics. As shown in *Figure 5A*, peak current in the Na$_V$1.7 IV relationship was 15.7 ± 1.3 nA (n = 31 ensembles), while that for Na$_V$1.8 was right shifted on the voltage axis by 10 mV, and reached only −2.6 ± 0.2 nA (n = 32). The time courses of individual currents (insets in *Fig. 5B, C*) reflected the known faster activation and inactivation of Na$_V$1.7. Our results also revealed large pharmacological differences between these currents. In *Figure 5B* an ascending series of lidocaine concentrations produced rapidly increasing, cumulative block of Na$_V$1.7 current. During washout, the reintroduction of drug-free ECS produced a rapid and complete recovery of the ensemble current. In a similar experiment on cells expressing hNa$_V$1.8 (*Fig. 5C*), each step-increase in [lidocaine] was punctuated by a transient washout of the local anesthetic. Nonetheless, a blocker dose–response relationship was obtained, because even after the highest lidocaine dose, washout was rapid and essentially complete within 20 s. From multiple experiments, mean lidocaine dose–response curves for hNa$_V$1.7 and hNa$_V$1.8 were obtained, and are presented superimposed in *Figure 5D* in addition to the dose–response curve for the related local anesthetic tetracaine (applied to cells expressing hNa$_V$1.8 only). The Hill fits for these curves (Figure 5D) gave lidocaine IC_{50} values of 2.67 ± 0.23 mM (n_H 1.5 ± 0.1, n = 10) for Na$_V$1.7 and 0.32 ± 0.01 mM (n_H 0.8 ± 0.02, n = 15) for Na$_V$1.8, revealing that Na$_V$1.8 had 10-fold greater sensitivity to this drug than Na$_V$1.7. For Na$_V$1.8, the tetracaine dose–response relationship lay to the left of that for lidocaine, as revealed by the IC_{50} of ~0.034 ± 0.006 mM (n_H 0.9 ± 0.1, n = 35). Thus, tetracaine was also

found to be about one order of magnitude more potent than lidocaine as a blocker of the $Na_V1.8$ channel. Success rates for the Na_V blocker assays ($I_{Na} > 300$ pA for the duration of the experiment) were on the order of 80%. R_{seal} ranged from 80 to 1200 MΩ (4–60 MΩ/20-cell ensemble), with higher averages for $Na_V1.8$ experiments (~400 MΩ/cell) as compared with $Na_V1.7$ experiments (~300 MΩ/cell).

hGABA$_A$R Chloride Current

$GABA_A$Rs conduct inward I_{Cl} (Cl^- efflux) at membrane potentials negative to the chloride equilibrium potential (calculated to be −70 mV for our standard ICS and ECS solutions). Thus, the application of increasing concentrations of GABA to a representative ensemble of HEK-hGABA$_A$ cells evoked a concentration-dependent increase in I_{Cl} (*Fig. 6A*, inset). Desensitization, that is, current decay in the maintained presence of the agonist, also increased in rate at higher [GABA]. The agonist dose–response plots (*Fig. 6A*) indicated an EC_{50} value of 4.8 ± 0.8 μM (n_H 2.4 ± 0.5, $n = 16$ ensembles) for GABA, compared with a value of 2.2 ± 0.1 μM (n_H 1.4 ± 0.1, $n = 16$ ensembles) for the synthetic agonist isoguvacine.

Allosteric modulation by benzodiazepines is perhaps the most important pharmacological characteristic of $GABA_A$Rs.[22] Therefore, to demonstrate this effect, we preincubated ensembles of cells with the modulators triazolam or diazepam for 1 min, followed by application of the EC_{20} concentration of GABA (determined separately to

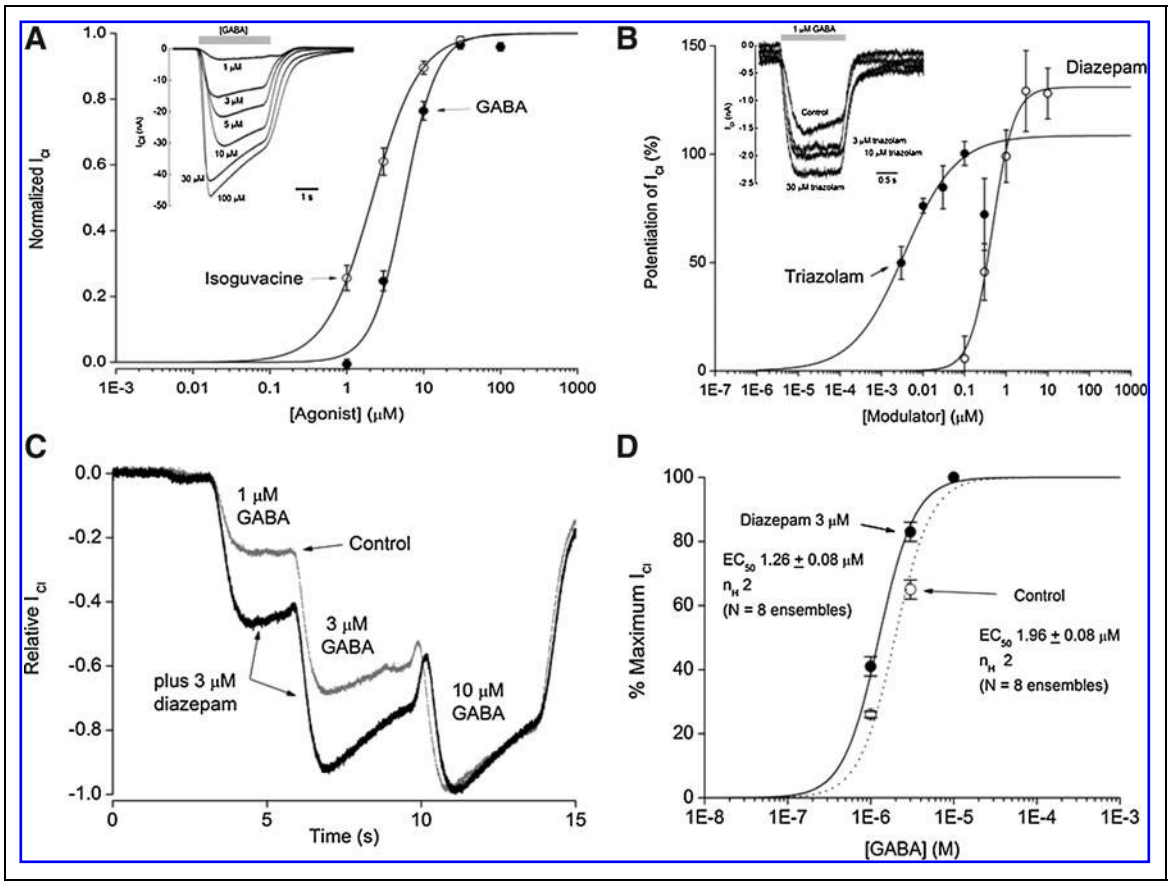

Fig. 6. HEK-hGABA$_A$ receptor chloride channel recordings. **(A)** Superimposed plots of I_{Cl} amplitude (at V_{hold} −80 mV throughout), normalized to the value at 30 μM, versus [agonist] for GABA, and isoguvacine. (*Inset*) IonFlux™ ensemble I_{Cl} traces evoked by applying an ascending series of [GABA] to one ensemble of cells, note the development of increasingly faster desensitization at higher concentrations of GABA. Hill fits to the dose–response curves yielded EC_{50} values of 4.8 ± 0.8 μM (n_H 2.4 ± 0.5, $n = 16$ ensembles) and 2.2 ± 0.1 μM (n_H 1.4 ± 0.1, $n = 16$ ensembles) for GABA and isoguvacine, respectively. **(B)** Superimposed dose–response plots for % potentiation of I_{Cl} evoked by EC_{20} [GABA], in the presence of increasing concentrations of diazepam and triazolam. The lines are Hill fits to the data with fitted parameters of EC_{50} 3.6 ± 1.9 nM (n_H 0.7 ± 0.3, $n = 4$ ensembles) for triazolam, and 0.50 ± 0.05 μM (n_H 1.6 ± 0.2, $n = 5$ ensembles) for diazepam. (*Inset*) Traces showing the increase of I_{Cl} evoked by an EC_{20} GABA concentration after adding 3–30 nM triazolam to the ECS (as indicated). **(C)** Superimposed raw traces from the cumulative GABA EC_{50} determination. Comparing the control ensemble current responses (dotted) and responses obtained during simultaneous exposures to GABA and 3 μM diazepam shows the potentiation of I_{Cl} at submaximal [GABA] (<10 μM). **(D)** Superimposed mean three-point dose–response curves from the control GABA applications (unmodulated) and 3 μM diazepam-exposed ensembles. From the Hill plot parameters shown on the graph, it can be seen that this dose of diazepam approximately doubled the apparent sensitivity to GABA. Note the absence of modulation at the highest [GABA] in **(C)** and **(D)**.

be 1 μM) in the continued presence of the modulator. *Figure 6B* (inset) shows that this protocol elicited modulator concentration-dependent increases in I_{Cl}. The calculated EC_{50} values were ~4 nM for triazolam and 500 nM for diazepam (*Fig. 6B*), implying that the affinity of triazolam for the modulator site exceeded that for diazepam by more than two orders of magnitude. Since the GABA EC_{20} response can be of low and variable amplitude, using this dose of GABA to stimulate the cells and measure allosteric modulation may lead to variability in the measured I_{Cl} enhancement, and a potentially more accurate method is to determine the modulation of the GABA dose–response curve. Because of the unique flow-through design of the IonFlux consumable, GABA concentrations can be increased very rapidly, enabling us to utilize cumulative GABA EC_{50} determinations to assess modulator efficacies. To illustrate this, *Figure 6C* shows a representative ensemble of GABA cells exposed sequentially to 1, 3, and 10 μM GABA in the presence and absence of 3 μM diazepam. Allosteric modulation of the GABA receptor can be observed as an increase in relative I_{Cl} in the presence of diazepam, for submaximal [GABA]. At 10 μM GABA, the saturated responses were fully activated and unavailable for modulation. These data, which were obtained in under 10 min of instrument time, were used to calculate the GABA EC_{50}, which shifted by about twofold to the left in the presence of 3 μM diazepam (*Fig. 6D*). The very fast readout demonstrated by this procedure is quite compatible with high-throughput screening for allosteric modulation. Success for GABA experiments (defined as $I_{Cl} > 1$ nA for the duration of the experiment) averaged 91% in three test experiments. R_{seal} varied from 60 to 400 MΩ/cell (3–20 MΩ/ensemble).

hNAChR Cation Current

NAChRs constitute another highly significant class of ligand-gated ion channels of interest to the pharmaceutical industry. As shown in *Figure 7C*, ensemble I_{Cat} conducted by α1 NAChRs activated and desensitized rapidly. *Figure 7A* shows the ACh concentration–response

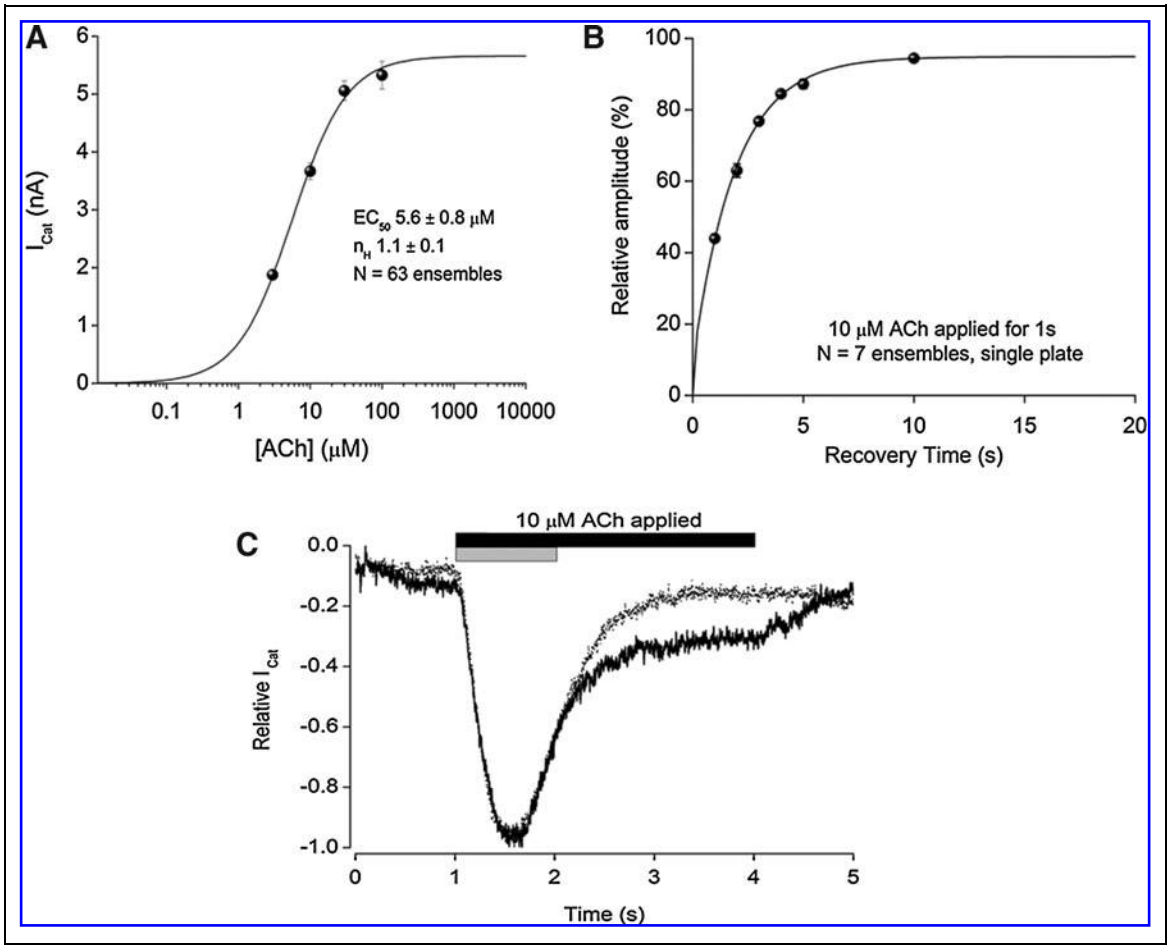

Fig. 7. hNAChR (α1) I_{Cat} recordings. **(A)** Plots of mean ensemble I_{Cat} amplitude (at V_{hold} −80 mV throughout) versus [ACh] for α1-hNAChR cells (see fitted Hill parameters on the graph) in the IonFlux instrument. **(B)** Recovery from desensitization in which I_{Cat} amplitude evoked by a 10 μM ACh application following closely after an identical initial exposure (Control response) is plotted against the intervening recovery time. The line is an exponential fit to the data ($\tau = 1.9 \pm 0.1$ s). **(C)** Superimposed recordings of 10 μM ACh-evoked I_{Cat} during agonist exposures of 1 s (dotted trace, gray bar) and 3 s duration (solid trace, black bar). hNAChR, human nicotinic acetylcholine receptor.

curve for this α1 receptor in which the EC_{50} was found to be 5.6 ± 0.8 μM (n_H 1.1 ± 0.1, n = 63 ensembles). The ability to exchange solutions rapidly is particularly important when studying fast-desensitizing channels such as NAChR to prevent the loss of channels from adversely affecting the accuracy of pharmacological experiments. Accordingly, we assessed the time course of recovery from desensitization induced by 10 μM ACh, using paired applications. *Figure 7B* shows peak ensemble I_{Cat} plotted against recovery time, revealing that in IonFlux experiments, NAChR desensitization recovered completely (despite minor rundown) within 10 s. Further evidence supporting the rapid removal of ACh appears in *Figure 7C*. It is known that α1 NAChRs develop a steady-state I_{Cat}, due to incomplete desensitization. Therefore, after abbreviating the ACh applications from 3 s to 1 s long, the effectiveness of agonist washout can be obtained from the amount of steady current observed. As indicated in the figure, steady-state current was clearly present during the 3-s ACh exposure, whereas during the briefer 1-s pulse of agonist, this current was completely absent, indicating that ACh washout was extremely fast.

DISCUSSION

We have shown how micron-sized channels can be molded in a polymeric substrate for incorporation into a consumable that enables the physical translation of cells and solutions under laminar flow. In the IonFlux plate, this is used for cell capture at recording sites, for voltage clamp, and for the application of drugs in high-throughput pharmacological experiments. This microfluidic approach greatly simplifies the mechanical design of our instrument, eliminating much of the complexity associated with other APC systems, even permitting experiments to be interrupted and restarted to facilitate fast assay development. A user-friendly operating environment avoids many of the intimidating technological demands associated with close emulation of conventional patch clamp recording. Temperature control, provided by a heating plate within the IonFlux instrument, together with the potential for optical access to voltage-clamped cells, is not replicated in other APC devices.

We also demonstrate the utility of a 12-well experimental unit, where a wide main channel acts as a low-pressure conduit for ECS plus cells from the inlet well reservoir, and conveys compound-containing solution from compound channel outlets to the cells captured in ERA recording sites (*Fig. 1C*). This 12-channel layout can be used for the generation of up to eight dose–response points for ion channel modulators, or if desired, for the delivery of different combinations of agents as in the cumulative GABA EC_{50} shift determined in *Figure 6*. Since ensemble voltage clamp recordings are made in duplicate using independent electrodes, it is likely that each zone on the plate will provide useable data. Indeed, over a diverse set of heterologously expressed ion channels, success rates averaged 80% or more, in keeping with the needs of high-throughput screening for drug discovery.

In common with other automated electrophysiology platforms, we work primarily with suspensions of small cultured cells in which human ion channels are expressed heterologously, as in the Millipore PrecisION range. Such cells have particular advantages in the drug-discovery arena since they are designed to purpose, and provide a large signal in virtually all cells.[23] In our particular experience, we advise selecting cells that do not aggregate tightly into colonies, and managing confluence carefully prevents contact inhibition from damaging ion channel expression: a maintained confluence of 80% consistently yields sufficient numbers of cells for experiments. Using these kinds of cells, we have obtained IonFlux validation data on prominent voltage- and ligand-gated ion channel targets. The $hK_V2.1$ channel is a potential target for increasing insulin secretion in diabetes.[24,25] The hERG K^+ channel is of obvious importance in safety pharmacology (as causal in acquired long QT syndrome) and in class III antiarrhythmics; for example, hERG blocking drugs, such as dofetilide, are licensed for treating atrial fibrillation.[26–28] Both $hNa_V1.7$ and $hNa_V1.8$ channels of the peripheral nervous system are recognized drug targets in the pain field,[29–31] while among ligand-gated channels, $hGABA_ARs$ are well known for involvement in CNS inhibition, being targeted widely in epilepsy, chronic anxiety, and insomnia.[22] Nicotinic receptors are of interest in many neuropsychiatric disorders ranging from neurodegeneration and schizophrenia, to Tourette's syndrome, epilepsy, and forms of addiction.[32]

Experiments performed with the IonFlux system readily reproduced the important electrophysiological features of these diverse channel types. For example, the $K_V2.1$ IV curve and voltage dependence presented in this report agreed well with published results[17,20] and, as shown in *Figure 3B*, were independently matched with manual patch-clamping data. More importantly, for an instrument aimed at high-throughput screening, we generated blocker IC_{50}s for TEA and quinidine of ~20 mM and 20 μM, respectively (*Fig. 3D*). For TEA, we used similar protocols using a traditional patch clamp setup and obtained an IC_{50} of 10 mM (n = 5, data not shown), while typical literature values are 4–5 mM. Literature values for quinidine IC_{50} measurements are 12 μM.[20,33,34] Our IonFlux values are close to manual patch clamp results, and are acceptably close to the published results as the cellular backgrounds and exact solutions used are not the same, which might differentially affect pharmacology. For the CHO-hERG channel, both the activation voltage dependence and rectification were similar to findings made by conventional patching in-house, and in the reference literature provided with the Millipore CHO cell line (CYL 3038). In addition, for standard blocker compounds terfenadine, cisapride, and quinidine that have widely differing affinities, IonFlux IC_{50} values were ~25 nM, 60 nM, and 1 μM, respectively. For comparison, accepted values of 44 nM, 13 nM, and 1 μM show good agreement.[35]

In the case of $hNa_V1.7$ and 1.8, direct comparisons of drug IC_{50} values have rarely been performed, probably due to difficulties in obtaining sufficiently high expression of the *SCN10A* gene ($Na_V1.8$) gene.[19] Ensemble currents for $hNa_V1.7$ and 1.8, both of which were expressed in HEK-293 cells, exhibited big differences in peak amplitude (*Fig. 5A*). Since cells were of relatively uniform physical dimensions between these two lines, such results point to a lower expression of $hNa_V1.8$. Despite this, our ensemble current amplitudes of 2–6 nA (average 3 nA) for $Na_V1.8$ were large enough for valid screening with this channel. Indeed, our results revealed a marked subtype specificity for resting-state lidocaine block between $hNa_V1.7$

(IC_{50} 3 mM) and 1.8 (IC_{50} 0.3 mM), making the latter 10-fold more sensitive to lidocaine than $hNa_V1.7$. These findings are strongly supported by available published lidocaine IC_{50} values of 1 mM for $Na_V1.7$ and 0.2 mM for $hNa_V1.8$.[36,37] For tetracaine acting against $hNa_V1.8$, other workers[38] obtained an IC_{50} of 11 μM, agreeing well with the present IonFlux IC_{50} of 34 μM and indicating that tetracaine affinity for this channel is also an order of magnitude greater than lidocaine affinity.

To evaluate IonFlux performance with respect to ligand-gated ion channels, we performed studies using $hGABA_AR$ and hNAChR (see the Methods section). The α1 $GABA_ARs$ predominate in the CNS where they mediate the hypnotic/sedative effects of benzodiazepines, and our experiments therefore focused on allosteric modulator effects against this target. As shown in *Figure 6*, GABA evoked concentration-dependent inward Cl^- currents that noticeably desensitized at higher doses, closely reproducing predicted behavior.[39] The measured EC_{50} values for GABA and isoguvacine were ~5 and 2 μM, while literature values from cells expressing identical subunits are 4 and 40 μM, respectively, showing excellent agreement.[11] Concentration-dependent I_{Cl} potentiation by benzodiazepines is illustrated by *Figure 6B*, with EC_{50} values for triazolam and diazepam of 4 nM and 500 nM, respectively, revealing strongly selective triazolam binding to the α1 $GABA_AR$. Available literature values, of 22 nM for triazolam and 160 nM for diazepam, are in reasonable agreement with our results and potencies with the same rank order.[11,40] The flow-through design employed in IonFlux allowed [GABA] to be changed very quickly around voltage-clamped cell ensembles, so cumulative GABA dose–response experiments could be used to determine allosteric modulator pharmacology (*Fig. 6C*). This unique feature of the IonFlux instrument revealed a twofold GABA EC_{50} shift in the presence of 3 μM diazepam (*Fig. 6D*), which was comparable to published results, with the additional benefit of having been obtained in under 10 runtime minutes.[40]

Further ligand-gating experiments exploring the characteristics of neuromuscular α1 NAChRs yielded an EC_{50} of ~6 μM for the native ligand (ACh), which is strongly supported by reference data (EC_{50}: 12 μM in the CYL 3052 data sheet; Millipore Corp.). Ensemble I_{Cat} recovered exponentially from desensitization with a time constant of ~2 s (*Fig. 7A*), reaching a plateau within 10 s of ACh applications. Moreover, the notable absence of steady-state I_{Cat} following brief ACh pulses underlines the advantages of fast solution exchanges available using microfluidics (*Fig. 7B, C*). Many investigators wait 30 s or more between agonist applications to ensure full desensitization recovery or use enzymatic digestion to eliminate trace levels of agonists between applications.[41,42]

In conclusion, we have shown that IonFlux ensemble currents reproduce the known voltage dependence and kinetics of multiple voltage- and ligand-gated ion channels with good success. The data included in the present report validate the IonFlux instrument as a drug-screening tool. Since automated electrophysiology is by now a mature field, these instruments are appearing increasingly in academic centers, serving to reduce the amount of personnel training required for screening data collection. IonFlux now provides the capability to perform pharmacology studies using ensemble recording (for increased consistency) in the individual academic lab where larger, higher cost instruments are not feasible. Our results indicate that this novel microfluidic approach will lead to still further increases in simplicity, cost effectiveness, and data consistency, supporting major utility of IonFlux for ion channel research and drug discovery. A number of important capabilities differentiate this approach from the existing platforms: compound exchange is fast and requires no wait times between compound applications, enabling a number of fast protocols to be executed synchronously across the recording plate; protocols can be paused and restarted during a run providing excellent flexibility for accelerated assay development; runtimes can be very short, such that potentiator assays for ligand-gated channels can be completed in under 10 min.

DISCLOSURE STATEMENT

No competing financial interests exist.

REFERENCES

1. Dunlop J, Bowlby M, Peri R, Vasilyev D, Arias R: High-throughput electrophysiology: an emerging paradigm for ion-channel screening and physiology. *Nat Rev Drug Discov* 2008;7:358–368.
2. Priest BT, Swensen AM, McManus OB: Automated electrophysiology in drug discovery. *Curr Pharm Des* 2007;13:2325–2337.
3. Southan A, James IF, Cronk D: Ion channels: new opportunities for an established therapeutic target class. *Drug Discov World* 2005;6(Summer 2005):17–23.
4. Wang X, Li M: Automated electrophysiology: high throughput of art. *Assay Drug Dev Technol* 2003;1:695–708.
5. Wood C, Williams C, Waldron GJ: Patch clamping by numbers. *Drug Discov Today* 2004;9:434–441.
6. Asmild M, Oswald N, Krzywkowski KM, Friis, S, Jacobsen RB, Reuter D, Taboryski R, Kutchinsky J, Vestergaard RK, Schroder RL, Sorensen CB, Bech M, Korsgaard MP, Willumsen NJ: Upscaling and automation of electrophysiology: toward high throughput screening in ion channel drug discovery. *Recept Channels* 2003;9:49–58.
7. Bruggemann A, Stoelzle S, George M, Behrends JC, Fertig N: Microchip technology for automated and parallel patch-clamp recording. *Small* 2006;2:840–846.
8. Fertig N, Blick RH, Behrends JC: Whole cell patch clamp recording performed on a planar glass chip. *Biophys J* 2002;82:3056–3062.
9. Schroeder K, Neagle B, Trezise DJ, Worley J, Ionworks HT: A new high-throughput electrophysiology measurement platform. *J Biomol Screen* 2003;8:50–64.
10. Finkel A, Wittel A, Yang N, Handran S, Hughes J, Costantin J: Population patch clamp improves data consistency and success rates in the measurement of ionic currents. *J Biomol Screen* 2006;11:488–496.
11. Hollands EC, Dale TJ, Baxter AW, Meadows HJ, Powell AJ, Clare JJ, Trezise DJ: Population patch-clamp electrophysiology analysis of recombinant GABAA alpha1beta3gamma2 channels expressed in HEK-293 cells. *J Biomol Screen* 2009;14:769–780.
12. John VH, Dale TJ, Hollands EC, Chen MX, Partington L, Downie DL, Meadows HJ, Trezise DJ: Novel 384-well population patch clamp electrophysiology assays for Ca2+-activated K+ channels. *J Biomol Screen* 2007;12:50–60.
13. Ly JQ, Shyy G, Misner DL: Assessing hERG channel inhibition using PatchXpress. *Clin Lab Med* 2007;27:201–208.
14. Mathes C, Friis S, Finley M, Liu Y: QPatch: the missing link between HTS and ion channel drug discovery. *Comb Chem High Throughput Screen* 2009;12:78–95.
15. Kiss L, Bennett PB, Uebele VN, Koblan KS, Kane SA, Neagle B, Schroeder K: High throughput ion-channel pharmacology: planar-array-based voltage clamp. *Assay Drug Dev Technol* 2003;1(1 Pt 2):127–135.
16. Chen C, Folch A: A high-performance elastomeric patch clamp chip. *Lab Chip* 2006;6:1338–1345.

17. Ionescu-Zanetti C, Shaw RM, Seo J, Jan YN, Jan LY, Lee LP: Mammalian electrophysiology on a microfluidic platform. *Proc Natl Acad Sci USA* 2005; 102:9112–9117.
18. Golden AP, Li N, Chen Q, Lee T, Nevill T, Cao X, Johnson J, Erdemli G, Ionescu-Zanetti C, Urban L, Holmqvist M: IonFlux: a microfluidic patch clamp system evaluated with human ether-a-go-go related gene channel physiology and pharmacology. *Assay Drug Dev Technol* 2011;9:608–619.
19. Zhao J, Ziane R, Chatelier A, O'Leary ME, Chahine M: Lidocaine promotes the trafficking and functional expression of Na(v)1.8 sodium channels in mammalian cells. *J Neurophysiol* 2007;98:467–477.
20. Immke D, Wood M, Kiss L, Korn SJ: Potassium-dependent changes in the conformation of the Kv2.1 potassium channel pore. *J Gen Physiol* 1999;113:819–836.
21. Zeng H, Penniman JR, Kinose F, Kim D, Trepakova ES, Malik MG, Dech SJ, Balasubramanian B, Salata JJ: Improved throughput of PatchXpress hERG assay using intracellular potassium fluoride. *Assay Drug Dev Technol* 2008;6:235–241.
22. Whiting PJ: The GABAA receptor gene family: new opportunities for drug development. *Curr Opin Drug Discov Devel* 2003;6:648–657.
23. Clare JJ, Chen MX, Downie DL, Trezise DJ, Powell AJ: Use of planar array electrophysiology for the development of robust ion channel cell lines. *Comb Chem High Throughput Screen* 2009;12:96–106.
24. Herrington J: Gating modifier peptides as probes of pancreatic beta-cell physiology. *Toxicon* 2007;49:231–238.
25. Herrington J, Sanchez M, Wunderler D, Yan L, Bugianesi RM, Dick IE, Clark SA, Brochu RM, Priest BT, Kohler MG, McManus OB: Biophysical and pharmacological properties of the voltage-gated potassium current of human pancreatic beta-cells. *J Physiol* 2005;567(Pt 1):159–175.
26. Sanguinetti MC, Jiang C, Curran ME, Keating MT: A mechanistic link between an inherited and an acquired cardiac arrhythmia: HERG encodes the IKr potassium channel. *Cell* 1995;81:299–307.
27. Smith PL, Baukrowitz T, Yellen G: The inward rectification mechanism of the HERG cardiac potassium channel. *Nature* 1996;379:833–836.
28. Witchel HJ: The hERG potassium channel as a therapeutic target. *Expert Opin Ther Targets* 2007;11:321–336.
29. Drenth JP, Waxman SG: Mutations in sodium-channel gene SCN9A cause a spectrum of human genetic pain disorders. *J Clin Invest* 2007;117:3603–3609.
30. Momin A, Wood JN: Sensory neuron voltage-gated sodium channels as analgesic drug targets. *Curr Opin Neurobiol* 2008;18:383–388.
31. Ogata N, Ohishi Y: Molecular diversity of structure and function of the voltage-gated Na+ channels. *Jpn J Pharmacol* 2002;88:365–377.
32. Romanelli MN, Gratteri P, Guandalini L, Martini E, Bonaccini C, Gualtieri, F: Central nicotinic receptors: structure, function, ligands, and therapeutic potential. *ChemMedChem* 2007;2:746–767.
33. He Y, Kang Y, Leung YM, Xia F, Gao X, Xie H, Gaisano HY, Tsushima RG: Modulation of Kv2.1 channel gating and TEA sensitivity by distinct domains of SNAP-25. *Biochem J* 2006;396:363–369.
34. Wang W, Hino N, Yamasaki H, Aoki T, Ochi R: KV2.1 K+ channels underlie major voltage-gated K+ outward current in H9c2 myoblasts. *Jpn J Physiol* 2002; 52:507–514.
35. Tao H, Santa Ana D, Guia A, Huang M, Ligutti J, Walker G, Sithiphong K, Chan F, Guoliang T, Zozulya Z, Saya S, Phimmachack R, Sie C, Yuan J, Wu L, Xu J, Ghetti A: Automated tight seal electrophysiology for assessing the potential hERG liability of pharmaceutical compounds. *Assay Drug Dev Technol* 2004;2: 497–506.
36. Sheets PL, Heers C, Stoehr T, Cummins TR: Differential block of sensory neuronal voltage-gated sodium channels by lacosamide [(2R)-2-(acetylamino)-N-benzyl-3-methoxypropanamide], lidocaine, and carbamazepine. *J Pharmacol Exp Ther* 2008;326:89–99.
37. Sheets PL, Jackson JO 2nd, Waxman SG, Dib-Hajj SD, Cummins TR: A Nav1.7 channel mutation associated with hereditary erythromelalgia contributes to neuronal hyperexcitability and displays reduced lidocaine sensitivity. *J Physiol* 2007;581(Pt 3):1019–1031.
38. Dekker LV, Daniels Z, Hick C, Elsegood K, Bowden S, Szestak T, Burley JR, Southan A, Cronk D, James IF: Analysis of human Nav1.8 expressed in SH-SY5Y neuroblastoma cells. *Eur J Pharmacol* 2005;528:52–58.
39. Bianchi MT, Botzolakis EJ, Haas KF, Fisher JL, Macdonald RL: Microscopic kinetic determinants of macroscopic currents: insights from coupling and uncoupling of GABAA receptor desensitization and deactivation. *J Physiol* 2007;584 (Pt 3):769–787.
40. Khom S, Baburin I, Timin EN, Hohaus A, Sieghart W, Hering S: Pharmacological properties of GABAA receptors containing gamma1 subunits. *Mol Pharmacol* 2006;69:640–649.
41. Malysz J, Anderson DJ, Gronlien JH, Ji J, Bunnelle WH, Hakerud M, Thorin-Hagene K, Ween H, Helfrich R, Hu M, Gubbins E, Gopalakrishnan S, Puttfarcken PS, Briggs CA, Li J, Meyer MD, Dyhring T, Ahring PK, Nielsen EO, Peters D, Timmermann DB, Gopalakrishnan M: *In vitro* pharmacological characterization of a novel selective alpha7 neuronal nicotinic acetylcholine receptor agonist ABT-107. *J Pharmacol Exp Ther* 2010;334:863–874.
42. Reitstetter R, Lukas RJ, Gruener R: Dependence of nicotinic acetylcholine receptor recovery from desensitization on the duration of agonist exposure. *J Pharmacol Exp Ther* 1999;289:656–660.

Address correspondence to:
Cristian Ionescu-Zanetti, PhD
Fluxion Biosciences, Inc.
384 Oyster Point Boulevard, Unit 6
South San Francisco, CA 94080

E-mail: cristian@fluxionbio.com